JOURNAL OF MATERIALS SCIENCE 39 (2004) 7341–7350

Effect of non-toxic corrosion inhibitors on steel in chloride solution

H. AKROUT
Unité de recherche Corrosion et Protections des Métalliques, BP 37, 1002 Tunis-Belvédère, Tunisie

L. BOUSSELMI
Laboratoire Eau & Environnement, Institut Nationale de Recherche Scientifique et Technique, BP 95 Hammam-Lif, Tunisie

E. TRIKI
Unité de recherche Corrosion et Protections des Métalliques, BP 37, 1002 Tunis-Belvédère, Tunisie
E-mail: ezzeddine.triki@enit.rnu.tn

S. MAXIMOVITCH, F. DALARD
Laboratoire d'Electrochimie et de Physico-chimie de Matériaux et d'interfaces, BP 75, 38402 Saint Martin D'Hères, France

The effect of certain non-toxic inhibitors on the corrosion resistance of ordinary steel in chloride solution (2×10^{-2} M NaCl) at pH 8 was studied by polarisation curves, Raman spectroscopy and the electrochemical quartz crystal microbalance (EQCM).

The inhibitors tested were ascorbic acid salts (SA) and 1-hydroxyethylidene, 1-diphosphonic acid salts (SHEDP), the results from addition inhibtors are carried in order to expect a combined effect.

The polarisation curves indicated an improvement in polarisation resistance with the addition of SA or SHEDP alone. In the presence of (SA + SHEDP), the inhibiting effect were further improved. Raman spectroscopy analyses confirmed the presence of a film formed by the two inhibitors at the iron electrode surface.

The individual behaviour of each inhibiteur was studied with EQCM for different chloride concentrations. The maximum of mass variation was obtained for a lower concentration in the case of SHEDP. The adsorption coverage was calculated. The Langmuir-Freundlich isotherm model is used to fit adsorption of the inhibitors. Interactions between adsorbed species were detected for SHEDP case.

For inhibitor mixture, detected mass attained plateau for low(er) inhibitors concentration mixture. At higher concentration, the mass quantity was smaller than that calculated from the sum of detected mass for each alone coumpound. However it provided better protection.

1. Introduction

Compounds used to inhibit corrosion of steel in contact with corrosive liquids generally contain nitrites or chromates [1]. However, the use of such inhibitors is becoming increasingly restricted in certain sectors, particularly in food and beverage applications, because of their toxicity and non-biodegradability.

Research efforts have therefore begun to focus on non-toxic, or green, corrosion inhibitors. Some recent studies have investigated the use of ascorbic acid in sulphate solutions [2]. Its effectiveness was demonstrated by B. Müller in the case of aluminium in a water butyric alcohol mixture [3]. Tanebe *et al.* [4] demonstrated the effectiveness of ascorbic acid in inhibiting corrosion of stainless steel in chloride solutions. They found that ascorbic acid acted by adsorbing at the metal surface and forming chelate compounds with the Fe^{2+} ions. Other studies have demonstrated that the inhibitor acts by preventing oxidation of Fe^{2+} to Fe^{3+} once a certain ascorbic acid concentration is reached [5].

Another non-toxic compound, 1-hydroxyethylidene, 1-diphosphonic acid (HEDP), is also considered to be a corrosion inhibitor [6].

The adsorption of certain non-toxic inhibitors at the metal surface has been studied using the electrochemical quartz crystal microbalance (EQCM) [7, 8].

The aim of the present study was to improve the corrosion resistance of ordinary steel in NaCl chloride solutions (2×10^{-2} M at pH 8) through the use of

TABLE I Composition of carbon steel

Elément	C	Si	Mn	P	S	Cr	Cu	Al	V	Fe
Composition	<0.07	<0.0002	0.38	0.021	0.004	<0.004	0.002	0.03	<0.004	residue

non-toxic corrosion inhibitors. The compounds tested were ascorbic acid salts and HEDP salts, plus a mixture of both. In fact, it may be important to complete the action of each inhibitor with other non-toxic products to obtain synergic effects.

The inhibiting effects of the experimental compounds were studied using various electrochemical techniques (polarisation curves and polarisation resistance (R_p)). Their effectiveness was assessed as a function of concentration. Raman spectroscopy was used to identify the elements present at the surface of the metal.

The EQCM was used to determine adsorption on the iron (and gold) electrode for each compound mentioned above, either alone or together.

2. Experimental conditions

2.1. Electrode material and electrochemical set-up

The experimental material was carbon steel. Its composition is given in Table I.

For the electrochemical study, the working electrodes, 1 cm^2 in area, were coated with a chemically inert resin. The surface was mechanically polished with SiC paper down to 1200 grit.

The reference electrode was a saturated calomel electrode (Hg_2Cl_2/Hg) and the auxiliary electrode was made of platinum.

The anodic polarisation curves were plotted with an EGG 273 potentiostat. The sweep rate was set at 15 mV/min.

2.2. Electrolyte and inhibitors

The test medium was an NaCl solution (2×10^{-2} M at pH 8). The non-toxic corrosion inhibitors used were as follows:

– L(+) ascorbic acid

This compound has two acidity constants: $pK_1 = 4.49$, $pK_2 = 12.72$ [9].

At pH 8, ascorbic acid is dissociated in the form of sodium ascorbate (SA). SA is in equilibrium with its conjugated form, dehydroscopic acid [4].

– 1-hydroxyethylidiene, 1-diphosphonic acid (HEDP).

This compound has 5 acidity constants: $pK_1 = 1.7$, $pK_2 = 2.47$, $pK_3 = 7.28$, $pK_4 = 10.29$, $pK_5 = 11.13$ [9].

At pH 8, three acidities are dissociated to give the HEDP salt (SHEDP).

3. Raman spectroscopy

The Raman spectra were measured *ex-situ* using a Dilor XY multichannel spectrometer equipped with a CCD (Charge-Coupled Device) detector, with the 514, 532 nm line of an argon laser as the excitation line. The laser line arrives vertically on the specimen. It is connected to an optical microscope with the lens maintained at magnification 50 for the pure compounds, and 100 for the surfaces immersed for 2 h at corrosion potential in the different electrolytes.

4. Electrochemical quartz crystal microbalance (EQCM)

4.1. Principle

The electrochemical quartz crystal microbalance (EQCM) detects frequency variations on the basis of the piezoelectric properties of the quartz.

The frequency variation is attributed to two terms, the first is due to the mass variation detected by quartz and the second is related to the increase in kinematic viscosity of the solution following addition of other substances [10, 12].

$$\Delta f = \Delta f_m + \Delta f_\nu$$

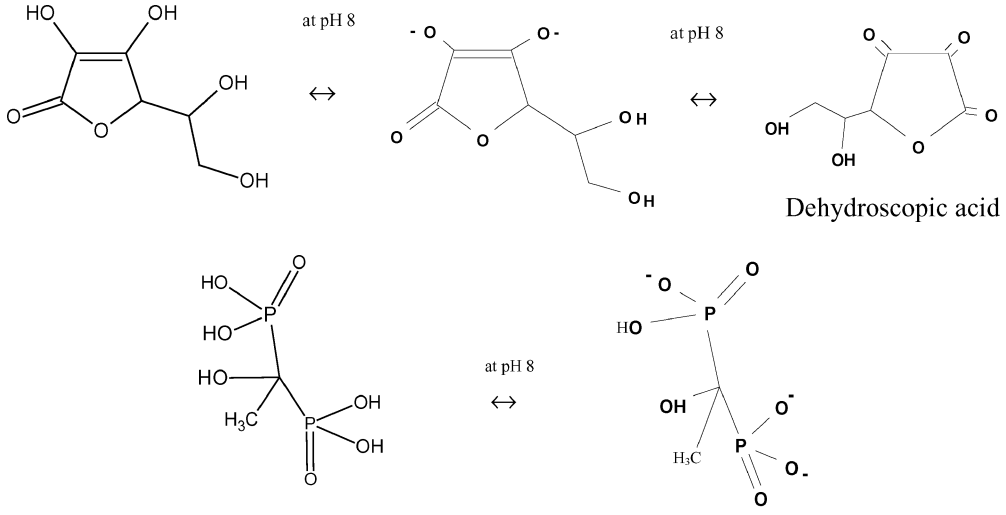

In the present study, the variation in kinematic viscosity during all additions of the inhibitor (SA or SHEDP) was disregarded. The frequency variation was only related to mass variations, and was in accordance with Sauerbrey's equation [10, 11]:

$$\Delta f = -2 f_0^2 \times \frac{\Delta m}{\sqrt{\mu_q \rho_q}}$$

Δf = frequency variation caused by deposit (Hz), f_0 = resonant frequency of quartz, Δm = mass variation linked to deposit ($g \cdot cm^{-2}$), μ_q = shear modulus of quartz ($2.947 \cdot 10^{11}$ $g \cdot cm^{-2} \cdot s^{-2}$), ρ_q = density of quartz (2.648 $g \cdot cm^{-2}$).

It may be noted that this mass variation is the global detected mass variation which involves mass variation in the vicinity of the electrode inside the electrolyte, and then represents much more than the chemisorbed mass at the electrode [7, 8].

4.2. Experimental set-up

The electrochemical cell was thermostatically controlled at 25°C and associated with an EQCM (Maxtek PM-710).

– *Gold electrode*: The piezoelectric quartz crystal, in the form of a thin wafer, was covered with a metallic gold coating 0.33 μm thick and 1.4 cm^2 in area. The natural oscillation frequency, called the resonant frequency or fundamental frequency f_0, of the quartz supplied by Neyco is 5 MHz. The frequency variation is:

$$\Delta f = -566 \times 10^5 \Delta m$$

This technique is sufficiently sensitive for adsorption measurements since the frequency variation of 1 Hz is able to detect 18 $ng \cdot cm^{-2}$ mass close to the electrode surface.

– *Iron electrode*: This was a gold electrode (quartz + gold deposit), covered with a 0.2 μm thick coating of iron, obtained by vacuum evaporation.

4.3. Experimental procedure

The NaCl solutions (chlorides) were always added first, followed by successive additions of SA or SHEDP. Thus, concentration "0" means that the tests were performed in pure water at pH 8, while the concentrations 10^{-4}, 10^{-3} and 2×10^{-2} refer to the NaCl solutions.

The inhibitors were added to the electrolyte in successive amounts of (no more than 5 mL), with the same chloride content after frequency stabilisation (less than 10 min) to an initial volume of 250 mL of pur water or NaCl solution at pH 8 (adjusted with NaOH). The pH value and chloride concentrations were always invariant.

The frequency variations was recorded immediately after the frequency step following the inhibitor addition. In this case, the frequency variations are attributed to only adsorption phenomena, corrosion phenomena which are negligible on these short periods.

The successive additions were being stopped when we attain the maximum inhibitor concentration, the frequency remain constant or increase after inhibitor addition.

5. Results and discussion

5.1. Polarisation curves

The anodic and cathodic polarisation curves for steel in the NaCl solution (2×10^{-2} M) with addition of SA only (Figs 1 and 2), SHEDP only (Figs 3 and 4) and mixtures of both inhibitors at different concentrations (Fig. 5) were obtained after 2 h at corrosion potential.

In the presence of SA (Fig. 1), the corrosion potential, E_{corr} was higher than in NaCl without ascorbate

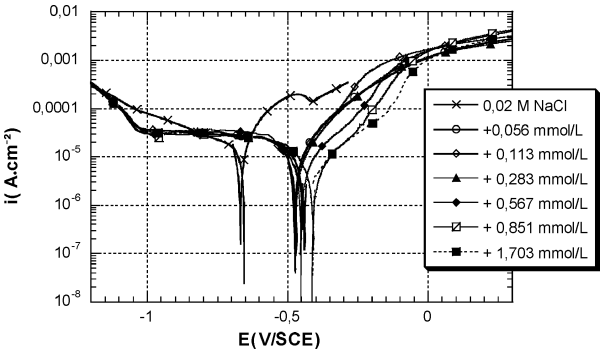

Figure 1 Cathodic and anodic polarisation curves for steel in the presence of different sodium ascorbate concentrations.

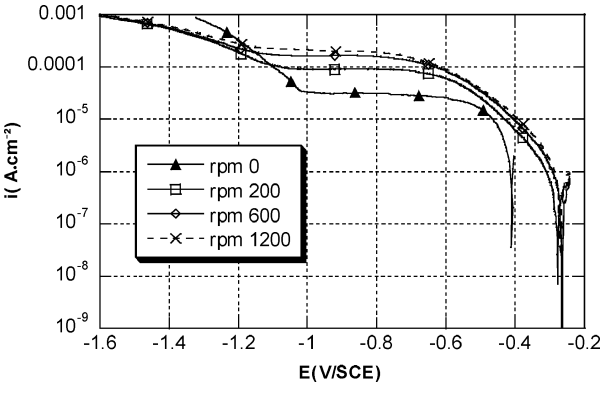

Figure 2 Influence of electrode rotation rate on plateau current for steel in the presence of 2×10^{-2} M NaCl, 1.7 $mmol \cdot L^{-1}$ SA.

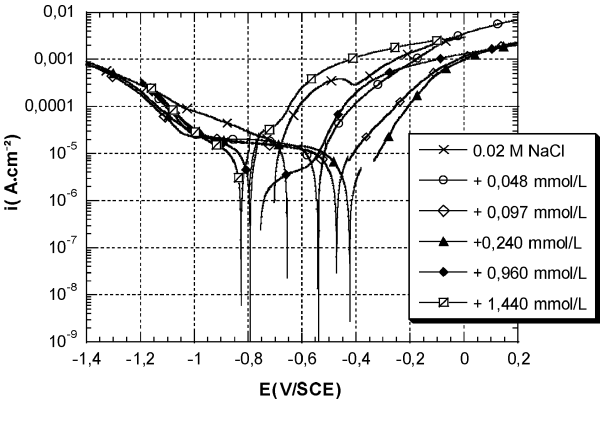

Figure 3 Cathodic and anodic polarisation curves for steel in the presence of different SHEDP concentrations.

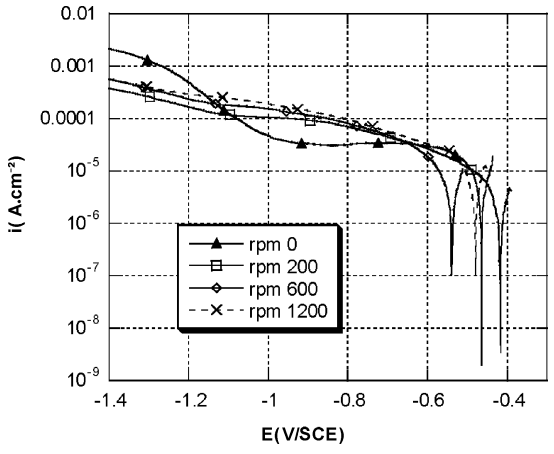

Figure 4 Influence of electrode rotation rate on plateau current for steel in the presence of 2×10^{-2} M NaCl, 0.24 mmol $\cdot$ L^{-1} SHEDP.

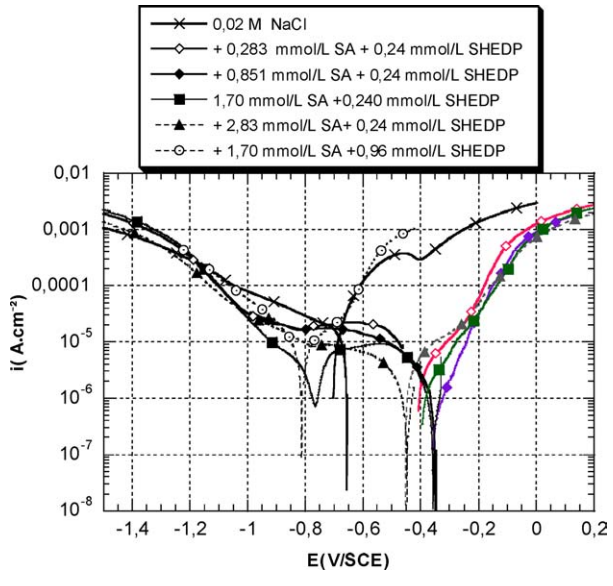

Figure 5 Cathodic and anodic polarisation curves for steel in the presence of different concentrations of SA and SHEDP.

(reference solution). It increased with the increase in inhibitor concentration. The anodic current density also dropped in the presence of SA. This result indicates that corrosion was slowed down when concentration of the inhibitor increases.

The cathodic polarisation curves exhibit a current density plateau -5×10^{-5} A $\cdot$ cm^{-2}, which is independent of the inhibitor concentration. This plateau might be related to oxygen diffusion. In order to determine the origin of this plateau, experiments were performed with different electrode rotation rates.

Fig. 2 shows the influence of the rotation rate on the cathodic plateau limiting current in chloride solution +1.7 mmol $\cdot$ L^{-1} SA. The current increased with rotation rate according to the Levich equation [13] and could be attributed to oxygen diffusion.

In the case of SHEDP (Fig. 3), E_{corr} (t = 2 h) increased with concentration in the presence of three lowest SHEDP concentrations. Nevertheless, in the presence of higher concentrations (0.96 and 1.44 mmol $\cdot$ L^{-1}), E_{corr} decreased compared with the reference solution (NaCl 2×10^{-2} M).

The anodic current densities also decreased with increasing SHEDP concentrations up to 0.96 mmol $\cdot$ L^{-1}. For higher concentrations (1.44 mmol $\cdot$ L^{-1}), the current density increased compared to the NaCl value. It seems that there is an optimum concentration near 0.96 mmol $\cdot$ L^{-1} and that in the presence of a high SHEDP concentration, an increase in the iron corrosion rate was observed.

In the presence of SHEDP, a limiting current density plateau, independent of SHEDP concentration, with a constant value of -2.07×10^{-5} A $\cdot$ cm^{-2} was observed. The experiments performed with different rotation rates (Fig. 4) indicate that contrary to SA solutions, this cathodic plateau current density did not vary with the rotation rate. This plateau could be related to SHEDP adsorption which did not appear to be limited by material transport [14].

In the case of NaCl + the SA-SHEDP mixture (Fig. 5), E_{corr} (t = 2 h) decreased in relation to the reference NaCl with a high SHEDP concentration and the anodic current was higher than without inhibitors. A low SHEDP concentration (C = 0.24 mmol $\cdot$ L^{-1}) was therefore used and the SA concentration was varied from 0.283 to 2.83 mmol $\cdot$ L^{-1}. The best corrosion protection was obtained for SA concentrations of 1.7 mmol $\cdot$ L^{-1} and 2.83 mmol $\cdot$ L^{-1}, as indicated by the anodic behaviour.

The cathodic polarisation curves for (NaCl + SA + SHEDP) were different. A plateau was observed only for SA concentrations of 0.283 and 0.851 (with 0.24 mmol $\cdot$ L^{-1} of SHEDP). For higher SA concentrations (2.17 and 2.83), a reduction peak instead of a plateau was observed.

The reduction peak situated at -0.50 V/SCE was more pronounced in the presence of 1.7 mmol $\cdot$ L^{-1} SA + 0.24 mmol $\cdot$ L^{-1} SHEDP. It may be related to the reduction of an oxidised species present at the electrode surface after 2 h immersion. This reduction peak was not observed during the cathodic potential sweep on a gold electrode in the same electrolyte. This reduced species was assumed to be related to ferric ions.

5.2. Polarisation resistance and inhibitor efficiency rate

The polarisation resistance (R_p) was estimated on the basis of the polarisation curves. The efficiency rate of the inhibitor ρ was calculated according to the following equation:

$$\rho = \left[(R_p)^{-1}_{reference} - (R_p)^{-1}_{i}\right] \Big/ (R_p)^{-1}_{reference}$$

with $(R_p)_{reference}$ = polarisation resistance without inhibitor.

$(R_p)_i$ = polarisation resistance with a concentration of inhibitor.

The polarisation resistance values and efficiency rates for each inhibitor concentration are given in Table II.

In NaCl (2×10^{-2} M) + SA, R_p increased with the SA concentration, while in the presence of SHEDP, R_p remained virtually constant for the low SHEDP concentrations and decreased for the high concentrations.

The efficiency rate was maximum in the case of high concentrations of SA alone.

TABLE II Polarisation resistance values (R_p) and effenciency rates (ρ)

[sodium ascorbate]/ mmol · L^{-1}	[sodium HEDP]/ mmol · L^{-1}	E_{corr} (mV/ECS) (t = 2 h)	R_p (kΩ · cm^{-2})	ρ^*
0	0	−673	1.77 ± 0.2	–
0.057	0	−477	2.99 ± 0.4	40.8
0.113	0	−447	3.12 ± 0.5	43.26
0.283	0	−472	2.64 ± 0.5	32.95
0.567	0	−439	4.23 ± 0.8	58.15
0.851	0	−410	6.58 ± 0.8	73.1
1.703	0	−439	4.75 ± 0.5	62.73
0	0.048	−522	3.38 ± 0.3	47.63
0	0.097	−480	3.5 ± 0.3	49.42
0	0.24	−432	3.27 ± 0.4	45.87
0	0.960	−792	2.73 ± 0.2	35.16
0	1.44	−832	2 ± 0.5	11.5
0.283	0.24	−407	12.58 ± 1	85.93
0.851	0.24	−351	20 ± 2	91.5
1.703	0.24	−397	21.36 ± 2	91.7
2.83	0.24	−447	11.11 ± 1.2	84.06
1.70 3	0.96	−813	2 ± 0.3	11.5

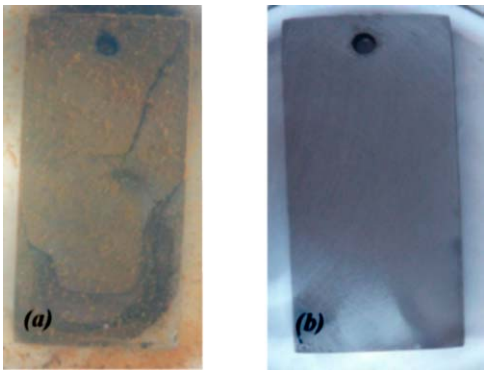

Figure 6 Photos of specimens immersed for 5 days (a) in 2 × 10^{-2} M NaCl (b) +1.7 mmol/L SA + 0.24 mmol · L^{-1} SHEDP.

The efficiency rate of SHEDP alone did not vary with the concentration.

For the mixture (SA + SHEDP), a high SA concentration and a low SHEDP value were required. If this condition was met, the variations in R_p and ρ indicated that the addition of the two inhibitors improved the corrosion protection of the steel in NaCl (2 × 10^{-2} M) solution.

In NaCl (2 × 10^{-2} M) solution, the best efficiency rate (91.7%) was obtained for concentrations of 1.703 mmol · L^{-1} sodium ascorbate + 0.24 mmoL^{-1} SHEDP.

5.3. Surface condition

The surfaces of the specimens immersed for 5 days without and with the inhibitor mixture are shown in Fig. 6. A comparison of the photos confirms the efficiency of the mixture of inhibitors in protecting the specimen.

5.4. *Ex-situ* Raman spectroscopy (SERS)

Fig. 7 shows the Raman spectra for the corroded surface of the reference specimen based on surface analysis after 2 h immersion in 0.02 M NaCl.

The peaks at around 248, 370 and 1312 cm^{-1} correspond to γ-FeOOH (lepidocrocite) [15–18].

The lines 226, 246, 293 and 1312 cm^{-1} correspond to α-Fe_2O_3 (hematite) [16–18].

The corroded surface of the reference specimen (0.02 M NaCl) after 2 h immersion was thus composed of a mixture of γ-FeOOH and α-Fe_2O_3.

This result is in agreement with data in the literature: the form γ-FeOOH is predominant in the case of short immersion times [19].

The spectrum corresponding to pure ascorbic acid is shown in Fig. 8a. The lines at around 1130, 1250 and 1300 cm^{-1} correspond to the vibrations of the ascorbic acid C–C and C–H bonds [20]. The line at around 840–887 cm^{-1} presents the (C–O–C) bond, while the (intense) line around 1650 cm^{-1} corresponds to the presence of two O–CH_2 groups found in ascorbic acid [20].

Analysis of the spectrum for the steel surface after 2 h immersion in NaCl 2 × 10^{-2} mol · L^{-1} + SA (Fig. 7b) shows that the line is again present around 1130 cm^{-1}. This result confirms the presence of a film containing SA C–C and C–H groups.

Analysis of the spectrum for pure HEDP (Fig. 8c) shows the presence of an intense line at around 1000 cm^{-1}. This line is characteristic of phosphate [20, 21]. It can be found on the Raman spectrum for the steel surface after 2 h immersion in NaCl 2 × 10^{-2} M + SHEDP (Fig. 8d) alone. This result provides proof of SHEDP adsorption.

The spectra obtained during analysis of the steel surface after 24 h immersion and 5 days immersion in NaCl 2 × 10^{-2} M in the presence of the mixture of the two inhibitors are shown in Fig. 7e and f. A few lines can be observed situated on the same wavelengths as those obtained in the case of pure ascorbic acid (around 800 and 1300 cm^{-1}).

The line corresponding to the phosphate is shifted towards 1000 cm^{-1}. This result may be attributed to the environment, which differed from that of the pure phosphate compound, or to an interaction between SA and SHEDP. The coexistence of the two compounds at

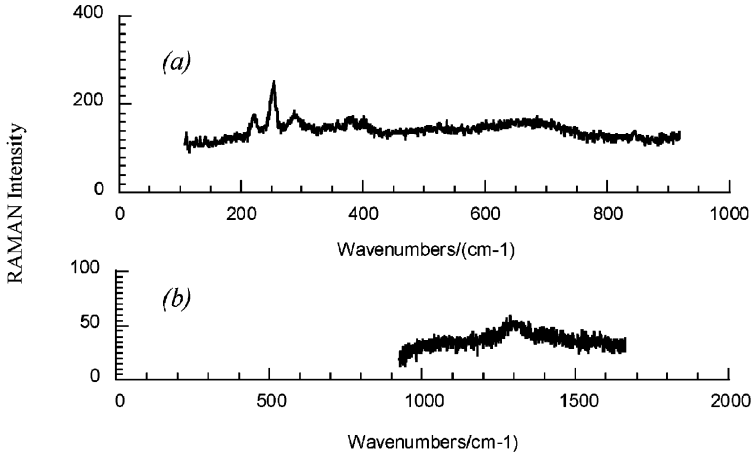

Figure 7 Ex-situ Raman spectra for the steel surface immersed in 2×10^{-2} M NaCl for 2 h. (a) on oxydes products (b) on the board.

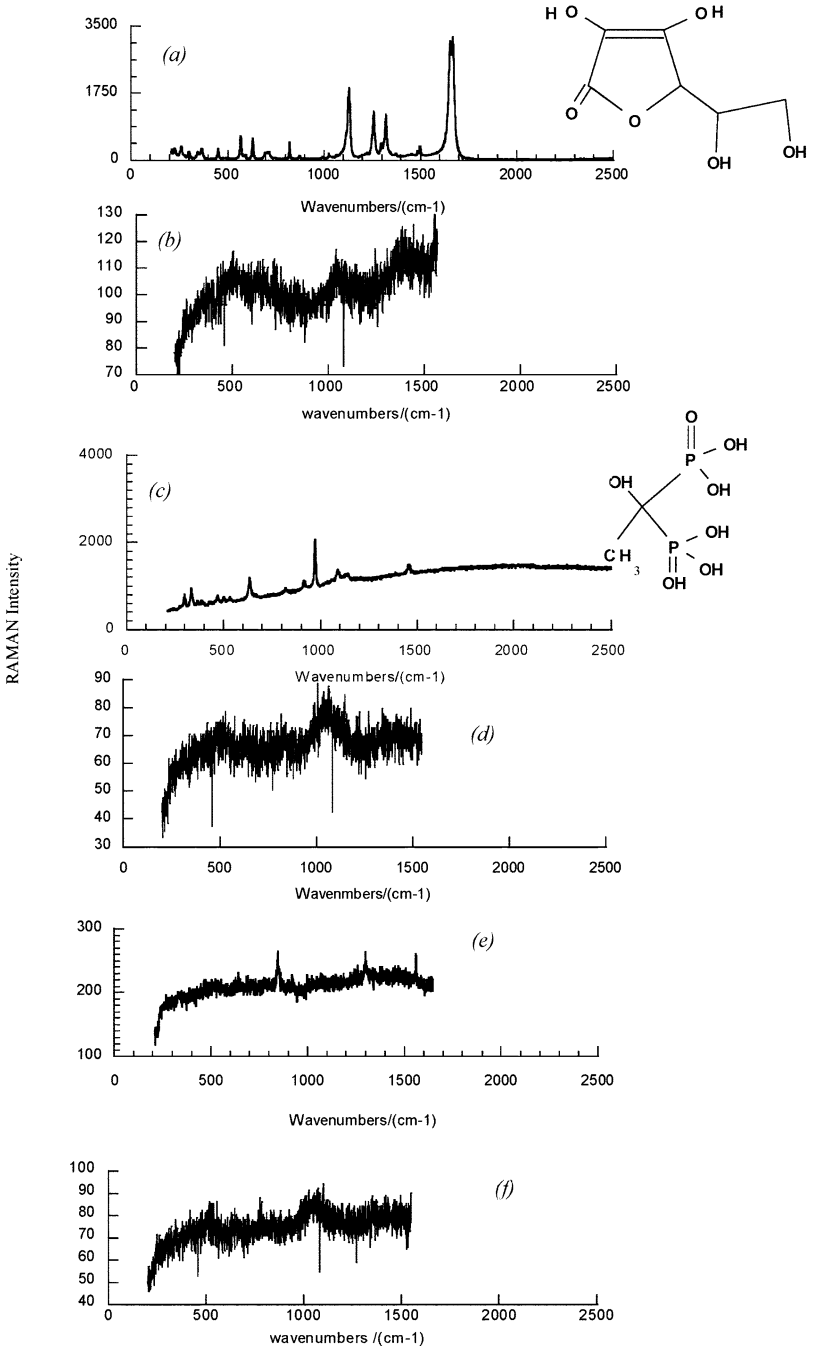

Figure 8 Raman spectra corresponding to (a) pure ascorbic acid (c) pure HEDP, for the steel surface immersed in 2×10^{-2} M NaCl + (b) 1.703 mmol · L^{-1} SA (24 h) + (d) 0.24 mmol · L^{-1} SHEDP (24 h) (e) + 1.703 mmol · L^{-1} SA + 0.24 mmol · L^{-1} SHEDP for 5 days (f) for 2 h.

the specimen surface indicates that the adsorbed film was composed of both inhibitors. The absence of lines corresponding to iron oxides on the specimen surfaces in the presence of the inhibitors confirms surface protection in these conditions.

In order to explain the mode of action of the inhibitors, SA and SHEDP adsorption was studied by measuring electrode mass variations using the electrochemical quartz crystal microbalance (EQCM). In this part of the study, the publications of Kern and Landolt [7, 8] were frequently consulted. These authors used an rEQCM (rotating electrochemical quartz crystal microbalance) to study adsorption on active or passive iron of benzoyl alkanoic acid with an amine (N-ethylmorpholine) or with NaOH. They compared it with the adsorption of the less bulky acid. Inhibitor adsorption was indicated by a mass variation. This result was interpreted as the displacement of the anions from the electrolyte into the volume considered by the microbalance by the inhibitor (adsorbed anions). Their results were interpreted according to a Langmuir–Freundlich adsorption model [7].

6. Electrochemical quartz crystal microbalance study

6.1. SA adsorption

The frequency variations measured on the iron (or gold) electrodes were recorded as a function of sodium ascorbate concentration and for different initial chloride concentrations. Sauerbrey's equation was used to convert these values to mass variations by comparison with the initial frequency in pure water at the same pH.

On iron, without chlorides, SA adsorption increased as a function of its concentration up to a plateau of 12 μg/cm^2 (Fig. 9a). At $[Cl^-] = 10^{-4}$ mol $\cdot$ L^{-1}, there was a slight initial mass variation, indicating negligible chloride adsorption, at 10^{-3}, this initial mass variation being of the order of 5×10^{-6} g $\cdot$ cm^{-2}. Then mass increased up a plateau indicating SA adsorption. With a high chloride concentration (2×10^{-2} mol $\cdot$ L^{-1}) the initial mass variation was very high (14 μg $\cdot$ cm^{-2}) then, mass variation was independent of SA additions indicating high chloride adsorption and low SA adsorption. It seems that the adsorbed chlorides (Cl^-) and hydroxides (OH^-) did not leave any room for the ascorbates to adsorb at the surface.

For chloride concentrations of 0, 10^{-4} and 10^{-3} mol $\cdot$ L^{-1}, the plateau was reached on the iron electrode for a SA concentration of the order of 5 mmol $\cdot$ L^{-1} (Fig. 9a). According to Landolt *et al.* [7, 8], the maximum mass variation is observed when a complete chemisorbed monolayer is formed at the electrode surface [7]. It may be noted that the mass corresponding to the plateau is much more higher than a mass of a monolayer. Assuming that the total mass variation is due to SA molecules, the number of SA molecules calculated without Cl^- was 5.7×10^{16} SA molecules/cm^2.

This number represents both the area and the volume in the immediate vicinity of the electrode measured by quartz frequency variation and also involves mass variation due to physically adsorbed molecules. It is dependent on the quartz resonant frequency [7] and is thus much greater than the concentration of a the first chemisorbed monolayer.

It should be noted that when the chloride ion concentration was increased, the total mass adsorbed on the iron electrode globally decreased. On the iron electrode and for all chloride concentrations, maximum adsorption was always reached in practically the same SA mass range.

With the gold electrode, similar results were obtained (Fig. 9b). However, the plateau was the same in the presence of different chloride concentrations.

By comparing these results with those of the electrochemical study and the Raman spectroscopy, the following conclusions can be drawn:

– Increasing the SA concentration improved the efficiency rate. If the SA concentration was increased above the adsorption maximum (5 mmol $\cdot$ L^{-1}), the adsorbed film mass was no longer modified, confirming the electrochemical results.

– The efficiency obtained with SA even in 2×10^{-2} M NaCl solution may be due to the fact that the electrolyte (in the electrochemical study) contained both chlorides and SA from the start of the experiment. The two species may have been adsorbed simultaneously, but always in the form of a monolayer. The hypothesis

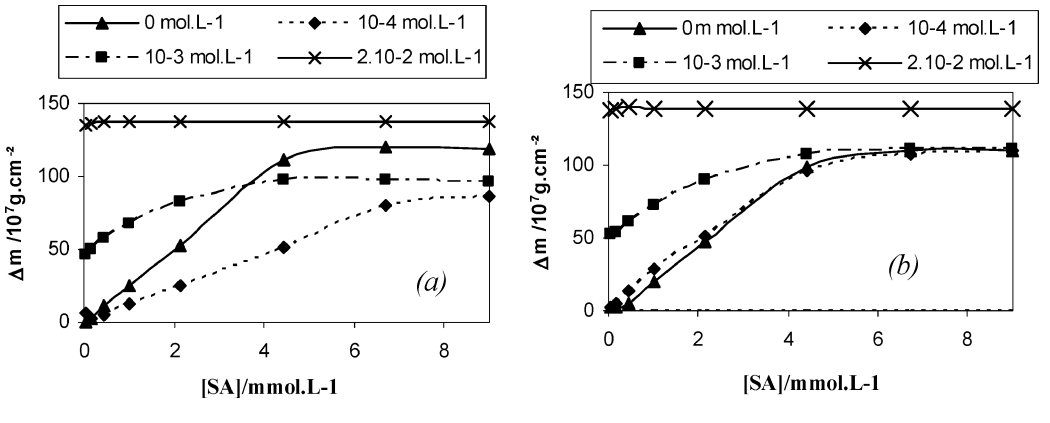

Figure 9 Influence of chloride concentration on adsorbed mass variation according to sodium ascorbate ion concentration, on (a) iron electrode (b) gold electrode.

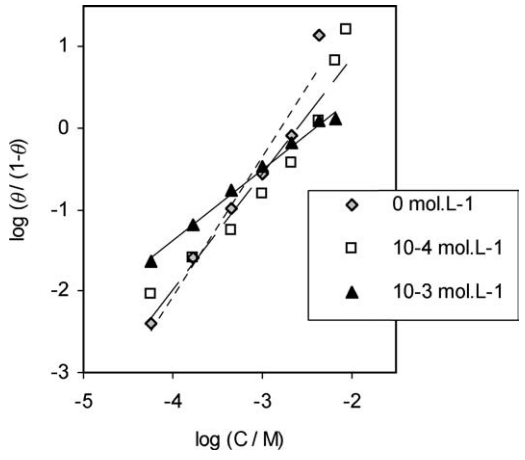

Figure 10 Curve adjusted according to Langmuir-Freundlich for sodium ascorbate adsorption on the iron electrode according to different chloride concentrations.

that inhibition took place solely through complexing in the solution was not confirmed by the Raman results. In fact, lines corresponding to SA were observed at the surface of the iron inhibited by SA alone.

The adsorption coverage θ on the quartz surface may be calculated as a fonction of inhibitor concentration according a to the formula:

$$\theta_{\Delta f} = \Delta f / \Delta f_{\max} \quad [7]$$

Δf is the frequency variation related to the considered SA concentration.

$\Delta f_{\max}$ frequency variation at the maximum [8]. It should de kept in mind that $\Delta f_{\max}$ is the sum of the frequency variations Δf related to the chlorides and the SA ions, assuming that chloride adsorption remains constant and is equal to its initial value.

The Langmuir-Freundlich isotherm describes a multisite adsorption on heterogeneous surfaces neglecting interactions between adsorbed species.

$$\theta = \frac{(KC)^{\mathrm{h}}}{1 + (KC)^{\mathrm{h}}} \quad [8]$$

with K adsorption constant,
h $(0 \leq h \leq 1)$ heterogeneity parameter for energy of sites.
$\log \theta/(1-\theta)$ varies as a function of $\log \mathrm{C}$ according to a linear relationship with a slope h, with $h = 1$ for

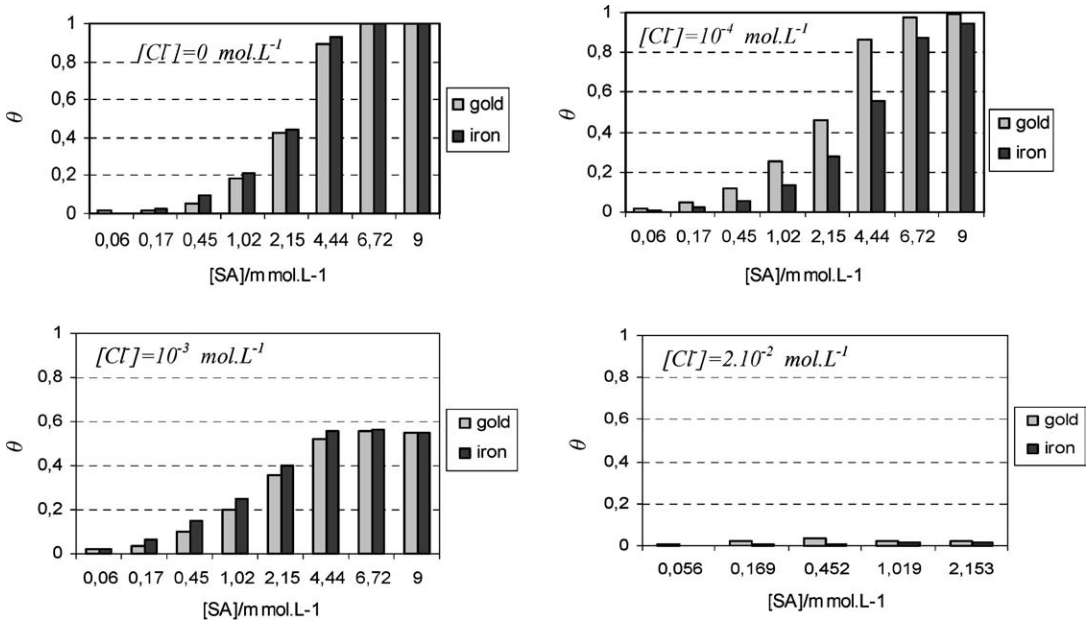

Figure 11 Influence of chloride ions on coverage of quartz by SA ions.

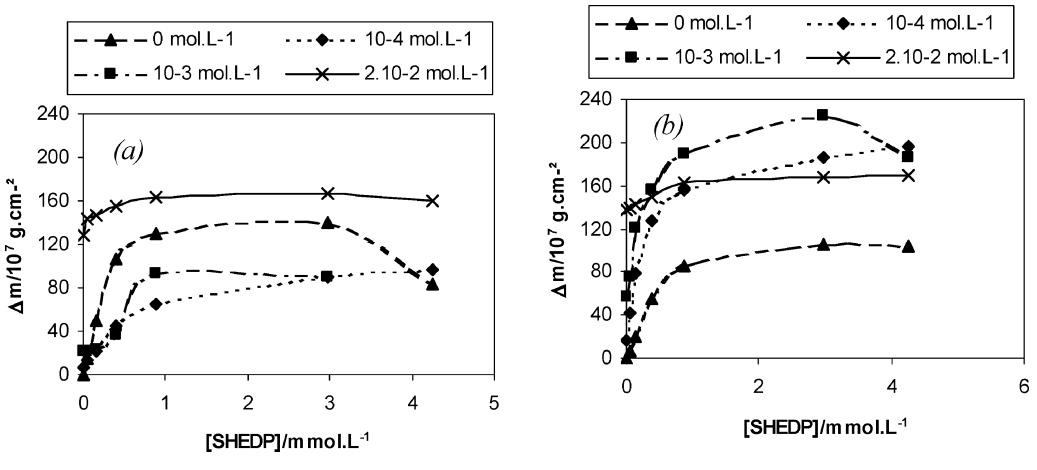

Figure 12 Influence of chloride concentration on adsorbed mass variation according to sodium HEDP ion concentration, on (a) iron electrode (b) gold electrode.

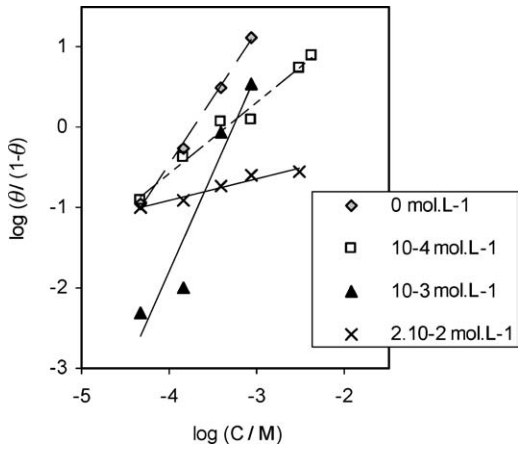

Figure 13 Curve adjusted according to Langmuir-Freundlich for SHEDP adsorption on the iron electrode according to different chloride concentrations.

a Langmuir isotherm when all sites have the same energy [5].

Fig. 10 shows the variation of $\log \theta/(1-\theta)$. The slope is close to 1, indicating that the active sites have the same adsorption energy [7].

In Fig. 11, the variation of SA coverage θ versus SA concentration is plotted on the iron electrodes for various chloride concentrations. Coverage increased with SA concentration until a maximum θ_{max} was reached, the maximum coverage θ_{max} decreased with the increase in chloride ion concentration, as illustrated in Fig. 11. A similar result was obtained for the gold electrode, confirming that the interfacial phenomena observed on the iron electrode were essentially due to adsorption rather than corrosion.

6.2. SHEDP adsorption

The influence of chloride concentration on adsorbed mass variation according to SHEDP ion concentration, on iron and gold electrode is illustrated in Fig. 12. The plateau of mass variation is reached for SHEDP concentration lower or of the order of 1 mmol $\cdot$ L^{-1} for the iron electrode (Fig. 12a), irrespective of chloride ion concentration.

Even in the presence of 2×10^{-2} M NaCl a mass increase is observed indicating simultaneous chloride and SHEDP adsorption both on the iron electrode and the gold electrode.

In the absence of chloride ions, for high concentration, a mass decrease occurred perhaps associated with desorption.

A similar result was obtained in the presence of chloride ions, for gold confirming the existence of an optimum concentration as for electrochemical results where high concentration promoted corrosion of the iron.

The number of adsorbed molecules calculated from the mass variation was 5.76×10^{16} on the iron electrode for a concentration of 1 mmol $\cdot$ L^{-1}, that is highly superior to the manolayer. However following Landolt *et al.* [7], this maximum is assumed to correspond to the formation of a monolayer of SHEDP [7].

Note the possibility of complexing between the HEDP and the bivalent cation Fe^{2+} [22].

$\log \theta/(1-\theta)$ varies linearly as a function of $\log C$ (Fig. 13). The slopes are different from 1, and vary with concentration, which may be indicative of a Langmuir-Freundlich's isotherm, with variable interactions.

SHEDP coverage on the iron electrodes was calculated as for SA. SHEDP coverage decreased with the increase in chloride ion concentration, as illustrated in Fig. 14. Coverage increased with the SHEDP concentration until it reached a maximum value. A similar result was obtained for the gold electrode.

The SHEDP coverage remained at levels of about 0.2 even in the presence a high NaCl concentration (2×10^{-2} M). This result is in agreement with the

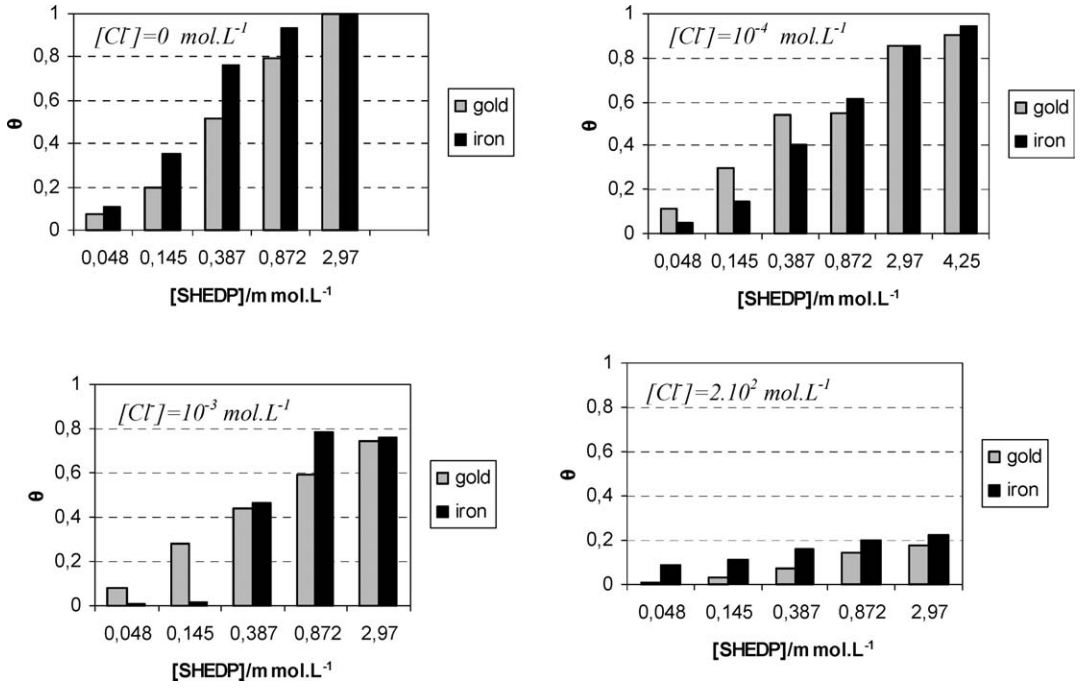

Figure 14 Influence of chloride ions on coverage of quartz by SHEDP ions.

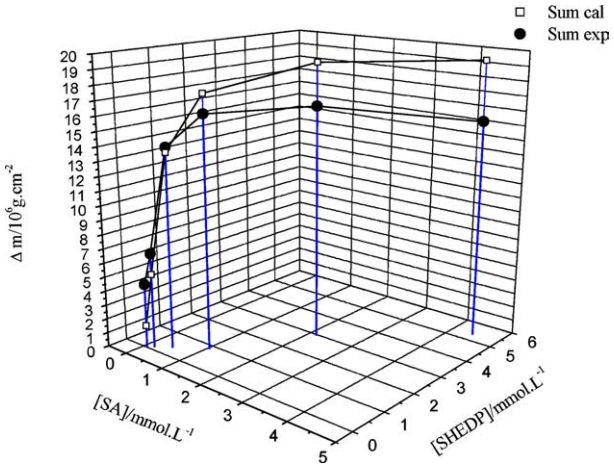

Figure 15 Comparison between experimental mass values and theoretical values (SA alone + SHEDP alone) corresponding to the SA + AHEDP mixture for the iron electrode in the absence of chloride ions.

Raman spectroscopy results (adsorbed film at surface contains line corresponding to steel in NaCl 2×10^{-2} M + SHEDP solution).

6.3. Adsorption of SA/SHEDP mixture

Fig. 15 illustrates the mass variation on the iron electrode as a function of the SA + SHEDP mixture concentration in the absence of chloride ions. In the case of a mixture composed of the two inhibitors SA and SHEDP, the mass variation was much greater as soon as the first additions of the inhibitor mixture were made.

The mass variation reached a plateau with low concentration of even SA and SHEDP. The layer is may be principally composed by SHEDP molecules than SA.

In high concentration, the experimental mass variation was smaller than the calculated value represented by adding the two mass variations of SA and SHEDP alone. This result may be attributable to interactions between SA and SHEDP. However, although it was lighter, the adsorbed film was more effective for corrosion protection according to the electrochemical study.

7. Conclusion

The anodic and cathodic polarisation curves were used to assess the efficiency of the inhibitors when used alone. SA was more efficient in higher concentrations. SHEDP was efficient in low concentrations. In fact, when a high concentration was used, corrosion of the steel was accelerated. The efficiency of each of the inhibitors in 2×10^{-2} M NaCl was improved in the presence of a mixture of Saand SHEDP.

Raman spectroscopy showed that the surface corroded in the chloride solution was formed of a mixture of γ-FeOOH and α-Fe_2O_3.

The adsorbed films in the presence of each of the inhibitors alone showed that SA and SHEDP acted by adsorption at the steel surface.

The surface immersed in the mixture with the optimum concentrations showed that the film formed at the iron surface was composed of the two inhibitors.

The electrochemical quartz crystal microbalance study showed the influence of chloride ions on adsorption of the two inhibitors. SA adsorption followed a Langmuir adsorption model with a maximum coverage reached at a concentration of 5 mmol $\cdot$ L^{-1}. SHEDP followed a Langmuir-Freundlich isotherm indicating interactions, with a maximum SHEDP adsorption reached at a concentration less than 3 mmol $\cdot$ L^{-1}.

In the presence of the solution of NaCl (2×10^{-2} M) + SA + SHEDP, the adsorbed film was lighter than the calculated value, but was more effective. This result can be explained by the interactions between SA and SHEDP.

An analogy between the results is indicative of the combined effect of the ascorbic acid and 1-hydroxyethylidiene, 1-diphosphonic in slowing down steel corrosion in NaCl solution.

References

1. I. L. ROZENFOLD, "Corrosion Inhibitors" (McGraw-Hill Internal Book Company, 1982).
2. R. SIMÕES GONÇALVES and L. DORNELLLES MELLO, *Corr. Sci.* **43** (2001) 457.
3. B. MÜLLER, *ibid.* **44** (2002) 1583.
4. I. SEKINE, Y. NAKAHATA and H. TANABE, *ibid.* **28** (1988) 987.
5. A. NIGAM, R. TRIPATHI, M. JANGID, K. DHOOT and M. P. CHACHARKAR, *ibid.* **30** (1990) 201.
6. C. GARCIA, G. GOURBIN, F. ROPITAL and C. FIAUD, *ibid.* **46** (2001) 973.
7. P. KERN and D. LANDOLT, *ibid.* **47** (2001) 589.
8. P. KERN and D. LANDOLT, *J. Electrochem. Soc.* **148**(6) (2001) B228.
9. E. P. SERGEANT and B. DEMPSY, Ionisation Constants of Organic Acids in Aqueous Solution, IUPAC CHEMICAL DATA SERIES–NO. 23.
10. P. KERN and D. LANDOLT, *Electrochimica Acta* **44** (2002) 1809.
11. G. SAUBERY, Zeitschrift für Physik **155** (1959) 206.
12. AN. HONG ZHOU, B. XIE and N. XIE, *Corr. Sci.* **42** (2000) 469.
13. J. P. DIARD, B. LE GORREC and C. MONTELLA, "Cinétique électrochimique" (Hermann, Paris, France, 1996).
14. P. AGARWAL and D. LANDOLT, *Corr. Sci.* **40**(4/5) (1998) 673.
15. W.-C. BEAK, T. KANG, H.-J. SOHN and YOUNG TAI KHO, *Electrochimica Acta* **46** (2001) 2321.
16. L. J. OBLONSKY and T. M. DEVINE, *Corr. Sci.*, **37**(1) (1995) 17.
17. PH. REFAIT, J.-B. MEMET, C. BON, R. SABOT and J.-M. R. GÉNIN, *ibid.* **45** (2003) 833.
18. J. GUI and T. DEVINE, *ibid.* **37**(8) (1995) 1177.
19. D. C. COOK, A. C. VANORDEN, J. J. CARPIO and S. J. OH, *Hyperf. Inter.* (1998) 319.
20. Y. GOURBEYRE, E. GUILMINOT and F. DALARD, *J. Mater. Sci.* **38** (2003) 1307.
21. R. S. COLE and R. FRESH, *J. Mol. Struct.* **643** (2002) 101.
22. I. FELHOSI, R. EKES, P. BARADLI, G. PALINKAS, K. VARGA and E. KALMAN, *J. Electroan. Chem.* **480** (2000) 199.

Received 17 July 2003
and accepted 29 April 2004